Constrained multispectrum analysis of CO_2–Ar broadening at 6227 and 6348 cm^{-1} [1]

D. Chris Benner, C.E. Miller, and V. Malathy Devi

Abstract: We report the first extensive experimental measurements of Ar-broadened half-width and pressure-induced shift coefficients, speed dependence parameters, and line mixing coefficients for the 30013←00001 and 30012←00001 bands of $^{16}O^{12}C^{16}O$ centered near 6227 and 6348 cm^{-1}, respectively. These parameters were determined from 15 self-broadened and six Ar-broadened CO_2 spectra recorded at room temperature with long absorption path lengths (25 to 121 m) using the McMath–Pierce Fourier transform spectrometer (FTS) at the National Solar Observatory. All 21 spectra were fit simultaneously using a multispectrum nonlinear least-squares technique. The line positions and line intensities were constrained to quantum mechanical expressions to obtain maximum accuracies in the retrieved parameters. Speed-dependent line shapes with line mixing (via the relaxation matrix formalism) were required to remove systematic errors in the fit residuals using only the Voigt profile. Remaining fit residuals were minimized by adjusting the half-width and pressure-induced shift coefficients of the overlapping 31113←01101 and 31112←01101 hot bands. We compare the Ar-broadening parameters with those recently determined for self- and air-broadening in the 30012←00001 and 30013←00001 bands and also with other Ar-broadening values from the literature, as appropriate.

PACS Nos: 32.70.–n, 32.70.Fw, 33.20.–t, 33.20.Ea, 33.70.–w, 33.70.Jg

Résumé : Nous présentons les premiers résultats expérimentaux complets de l'étalement de la demi- largeur de ligne dû à la présence d'argon et des coefficients de déplacement de ligne induits par la pression, les paramètres de dépendance en pression et les coefficients de mélange de ligne pour les bandes de 30013←00001 et 30012←00001 du $^{16}O\ ^{12}C^{16}O$ centrés près de 6227 et 6348 cm^{-1} respectivement. Nous avons déterminé ces paramètres à partir de 15 spectres de CO_2 auto-élargis et six spectres avec élargissement causé par la présence d'argon, enregistrés à température de la pèce et avec les longs chemins d'absorption (25 à 121 m) du spectromètre McMath-Pierce à transformée de Fourier (FTS) du National Solar Observatory. Nous avons simultanément ajusté mathématiquement l'ensemble des 21 spectres à l'aide d'une méthode de moindres carrés multispectrale et non linéaire. Les positions et intensités de ligne ont été ajustées aux expressions de la mécanique quantiques pour garantir un maximum de précision des paramètres extraits de l'analyse. Nous avons dû inclure une dépendance en vitesse de la forme des lignes et un mélange de lignes (via le mécanisme de la matrice de relaxation) afin d'éliminer les erreurs systématique dans les ajustements résiduels utilisant des profils de Voigt purs. Les autresajustements résiduels ont été minimisés en utilisant la demi-largeur et les coefficients de déplacement de ligne induit par la pression des bandes chaudes se recouvrant 31113←01101 et 31112←01101. Nous comparons nos résultats d'élargissement causés par l'argon avec ceux obtenus récemment d'élargissement par l'air dans les bandes 30012←00001 et 30013←00001, ainsi qu'avec d'autres résultats dans la littérature concernant un élargissement par l'argon.

[Traduit par la Rédaction]

1. Introduction

Accurate line positions, absolute line intensities, self- and air-broadened half-width and pressure-induced shift coefficients for transitions of the 30012←00001 and 30013←00001 bands of $^{16}O^{12}C^{16}O$ have recently been reported [1–7]. Line mixing and speed dependence for the majority of the transitions in these bands were also determined [4, 5] to minimize most of the systematic residuals using a constrained multispectrum fitting technique [8]. These data provide the CO_2 spectroscopic reference standards necessary to retrieve mixing ratios with uncertainties approaching 0.3% from observations to be made by the Orbiting Carbon Observatory (OCO) [9] and the Total Column Carbon Observing Network (TCCON) [10]. The primary goal of the present study is to provide accurate CO_2 spectroscopic reference standards for Ar-broadening parameters in the same spectral regions (6280 to 6395 cm^{-1} and 6120 to 6280 cm^{-1}) studied in [4, 5].

Despite the extensive investigations of CO_2–Ar infrared spectra [11–32], there have been only three previous studies of Ar-broadened CO_2 spectra in the region 6100–6400 cm^{-1}. Valero and Suarez [11] determined the pressure-broadened half-width coefficients for the 30012←00001 band from 0.075 cm^{-1} resolution Fourier transform spectrometer data, using the equivalent width method to analyze each spectral line for each sample condition. They measured the Ar-

Received 3 October 2008. Accepted 10 November 2008. Published on the NRC Research Press Web site at cjp.nrc.ca on 14 July 2009.

D.C. Benner[2] and V.M. Devi. The College of William and Mary, Box 8795, Williamsburg, VA 23187-8795, USA.
C. Miller. Jet Propulsion Laboratory, California Institute of Technology, 4800 Oak Grove Drive, Pasadena, CA 91109, USA.

[1]This article is part of a Special Issue on Spectroscopy at the University of New Brunswick in honour of Colan Linton and Ron Lees.

[2]Corresponding author (e-mail: dcbenn@wm.edu).

Table 1. Summary of experimental conditions of the CO_2 and CO_2–Ar spectra.

Pure CO_2			CO_2 in argon			
Temp (K)	Pressure[a] (torr)	Path length (m)	Temp (K)	Pressure (torr)	CO_2 volume mixing ratio	Path length (m)
293.99	896.84	49.00	294.41	902.17	0.0617	121.18
293.68	556.56	49.00	293.84	621.41	0.0892	121.18
293.49	252.42	49.00	293.70	248.87	0.0625	121.18
293.09	52.14	49.00	293.47	100.14	0.0619	121.18
293.89	450.93	24.94	294.37	550.50	0.0500	24.94
293.88	101.95	24.94	294.18	50.06	0.0505	24.94
293.94	26.10	24.94				
294.05	11.04	24.94				
293.37	252.01	2.46				
294.37	94.65	2.46				
293.58	75.27	2.46				
294.09	50.70	2.46				
292.79	30.31	2.46				
293.57	25.61	2.46				
293.38	9.973	2.46				

[a]Pure (natural) CO_2 samples (volume mixing ratio = 1 with 0.9842 $^{16}O^{12}C^{16}O$). 1 atm = 101.3 kPa = 760 torr.

broadened half-width coefficients at 197, 233, and 294 K, although they did not determine the temperature dependence exponents of the half-width coefficients. Suarez and Valero [12] did a similar study for the 30013←00001 band. Nakamichi et al. [30] determined Ar-broadened half-width coefficients for the R0, P8, P16, P26, and P38 of the 30013←00001 band from spectra recorded with a diode laser based continuous wave (cw) cavity ring-down spectrometer. They employed a Voigt function in their analysis. Recently, room temperature air- and Ar-broadened half-width coefficients were reported by Li et al. [32] for 11 R-branch transitions (R0–R20) in the 30012←00001 band. Their data were obtained with a photo acoustic spectrometer in conjunction with a high-resolution tunable diode laser, and analysis was performed employing a standard Voigt line shape on individual spectral lines.

Line mixing effects in CO_2–Ar spectra have been reported by several investigators using energy corrected sudden (ECS) calculations [e.g., 18, 19, 21, 23, 24]. In particular, Ozanne et al. [21] reported experimental and theoretical results on CO_2–Ar spectra in the ν_3 and $3\nu_3$ bands. At pressures of 100–1000 bars (1 bar = 100 kPa) they observed interbranch (R↔P) line mixing on the spectral shapes. Filippov et al. [18] analyzed the absorption coefficients in the $3\nu_3$ band of CO_2 at pressures up to 146 bar using two theoretical line-mixing calculations within the impact approximation. Rachet et al. [16] studied line mixing effects in the 20001←01101 and 12201←01101 Q branches located near 2130 and 2093 cm^{-1} of the spectra of CO_2, in mixtures with N_2, O_2 and Ar.

To our knowledge the only studies that have been reported on the temperature dependence exponents for CO_2–Ar collision broadening coefficients are by Brownsword et al. [15] and Wooldridge et al. [20]. Wooldridge et al. [20] used a cw lead-salt diode laser and studied the R48-R52 transitions of the ν_3 band of CO_2 in the temperature range of ∼ 297 – 2293 K. They compared their CO_2–Ar half-width coefficients with prior experimental investigations and also reported a value of 0.61 as the temperature dependence exponent, which is quite different from the value of 0.88 ± 0.18 published by Brownsword et al. [15].

In this paper, accurate measurements of Ar-broadened half-width and Ar-induced pressure shift coefficients are reported for the 30012←00001 and 30013←00001 bands of $^{16}O^{12}C^{16}O$ for transitions up to $J'' = 62$. In addition to the broadening parameters, line mixing coefficients via the relaxation matrix formalism [33] and speed dependence were required to remove most of the systematic residuals from the least-squares fits. A critical difference between the present study and the works of Valero and Suarez and Suarez and Valero [11, 12] is that the present study employed a multispectrum analysis that fit simultaneously all experimental spectra over the entire spectral interval for each band (6120 to 6280 cm^{-1} for the 30013←00001 band and 6280 to 6395 cm^{-1} for the 30012←00001 band), rather than independently measuring the half-width and pressure-induced shift coefficients for each spectral line in every spectrum and regressing these individual results to obtain the final coefficients. A modified multispectrum nonlinear least-squares retrieval procedure, including the capability to constrain spectral line parameters such as positions and intensities, enabled us to minimize the measurement uncertainties of the various retrieved parameters. Details of the retrieval algorithm will be provided in a separate article by Benner et al. [34].

2. Experimental

The experimental procedure has been described in [1–5]. All data were recorded at 0.01 cm^{-1} resolution over the 3800–8500 cm^{-1} range, using the McMath–Pierce Fourier transform spectrometer of the National Solar Observatory on Kitt Peak, Arizona. To ensure consistency with our previous work, the same 15 spectra used to determine CO_2 self-broadening parameters in refs. 4 and 5 were included in the present analysis. These 15 spectra were recorded at

Fig. 1. Multispectrum fit of self- and Ar-broadened CO_2 spectra from 6280 to 6395 cm^{-1}. (*a*) Twenty-one experimental spectra recorded at ~0.01 cm^{-1} resolution using the Fourier transform spectrometer at the National Solar Observatory on Kitt Peak. The set includes 15 high-purity CO_2 spectra in a natural mix of isotopologues and six CO_2 + Ar spectra recorded near room temperature. Positions of transitions included in the fit are indicated by tick marks shown at the top of panel (*a*). Each spectrum is normalized to the highest signal in the fitted interval. The 100% absorption line is shown by dotted line at the bottom of panel (*a*). (*b*) The corresponding weighted residuals (observed minus calculated on an expanded vertical scale) using a Voigt profile modified with speed dependence and line mixing (via relaxation matrix). (*c*) The weighted residuals for the six Ar-broadened CO_2 spectra. Panels (*b*) and (*c*) illustrate that appropriate weights were used for each of the 21 spectra in the analysis. The residuals shown in panel (*c*) are identical to the fit residuals for the six Ar-broadened spectra in (*b*) and are shown separately for illustrative purpose only.

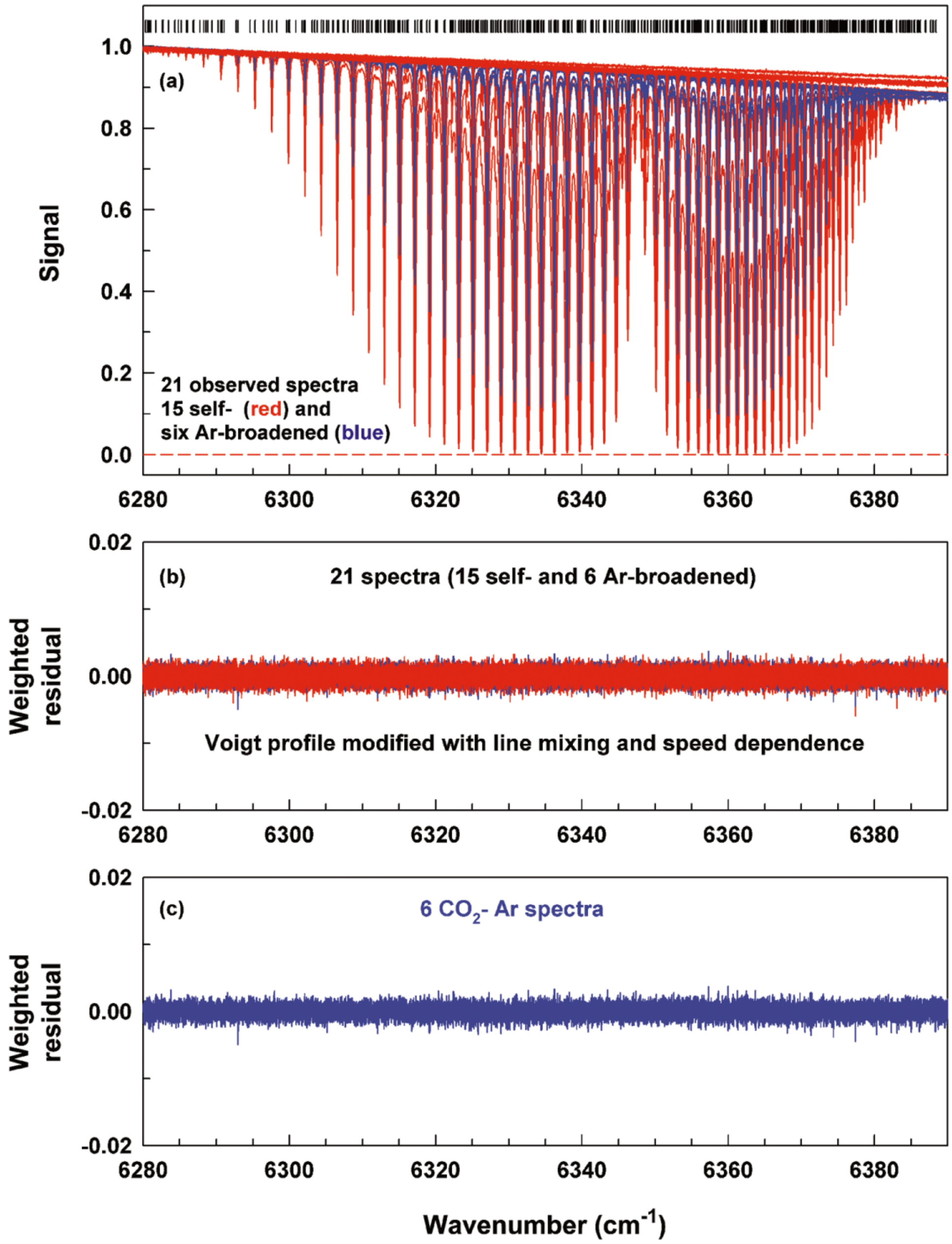

room temperature (~294 K), with path lengths ranging from L = 2.46 to 49 m. The self-broadened spectra were augmented by six Ar-broadened CO_2 spectra, also recorded at room temperature, using the same experimental set up. The volume mixing ratios of CO_2 in the CO_2–Ar spectra ranged from 0.05 to 0.09. Table 1 summarizes the experimental conditions for all spectra used in the present analysis.

3. Data retrieval and analysis

The multispectrum retrieval procedure used in the present work is the same used previously to determine accurate line positions, absolute intensities, self- and air-broadened half-width and pressure-shift coefficients, self and air line-mixing coefficients, and speed dependence for transitions up to J'' = 60 in the 30012←00001 and 30013←00001 bands [4, 5].

Table 2. Ar-broadened half-width and pressure-induced shift coefficients and speed dependence in the 30012←00001 band of $^{16}O^{12}C^{16}O$.

Line	Position[a]	b_L^0(Ar)[b]	Unc. (%)	δ^0(Ar)[c] unc.	SD[d]	Unc. (%)
P62e	6 285.888 62	0.041 76	6.39	–0.011 47 (268)	0.1	
P58e	6 290.650 27	0.052 68	2.82	–0.013 15 (145)	0.1	
P56e	6 292.996 79	0.047 03	1.85	–0.007 76 (85)	0.1	
P54e	6 295.319 76	0.048 17	1.27	–0.010 15 (59)	0.1	
P52e	6 297.618 70	0.047 47	0.88	–0.009 78 (41)	0.1	
P50e	6 299.893 14	0.048 78	0.64	–0.011 02 (30)	0.1	
P48e	6 302.142 65	0.049 71	0.46	–0.008 60 (22)	0.1	
P46e	6 304.366 82	0.050 17	0.36	–0.009 10 (17)	0.1	
P44e	6 306.565 25	0.051 02	0.27	–0.008 86 (13)	0.1	
P42e	6 308.737 56	0.051 48	0.21	–0.008 81 (10)	0.1	
P40e	6 310.883 40	0.051 93	0.17	–0.008 48 (8)	0.1	
P38e	6 313.002 45	0.052 19	0.15	–0.008 80 (10)	0.094	1.7
P36e	6 315.094 37	0.052 88	0.13	–0.008 31 (8)	0.089	1.8
P34e	6 317.158 87	0.053 24	0.13	–0.008 30 (7)	0.093	1.6
P32e	6 319.195 68	0.054 02	0.11	–0.008 37 (7)	0.105	1.3
P30e	6 321.204 52	0.054 25	0.11	–0.008 13 (6)	0.085	1.9
P28e	6 323.185 16	0.055 20	0.11	–0.007 93 (6)	0.100	1.4
P26e	6 325.137 35	0.056 21	0.11	–0.008 01 (5)	0.103	1.3
P24e	6 327.060 90	0.057 06	0.11	–0.007 70 (5)	0.103	1.3
P22e	6 328.955 59	0.058 42	0.10	–0.007 58 (5)	0.114	1.1
P20e	6 330.821 24	0.059 76	0.10	–0.007 48 (5)	0.127	0.9
P18e	6 332.657 69	0.060 74	0.10	–0.007 05 (5)	0.120	1.1
P16e	6 334.464 79	0.062 52	0.14	–0.006 83 (9)	0.139	0.9
P14e	6 336.242 38	0.063 94	0.09	–0.006 84 (5)	0.137	0.9
P12e	6 337.990 36	0.065 59	0.09	–0.006 80 (5)	0.138	0.8
P10e	6 339.708 60	0.066 74	0.09	–0.006 25 (6)	0.125	1.0
P08e	6 341.397 01	0.068 80	0.10	–0.006 02 (6)	0.134	0.9
P06e	6 343.055 51	0.070 66	0.17	–0.005 40 (12)	0.121	1.0
P04e	6 344.684 03	0.072 91	0.14	–0.005 92 (10)	0.112	1.2
P02e	6 346.282 51	0.076 85	0.18	–0.004 15 (17)	0.129	1.0
R00e	6 348.623 82	0.080 52	0.31	–0.002 63 (32)	0.100	2.1
R02e	6 350.147 05	0.074 21	0.13	–0.004 39 (12)	0.122	1.0
R04e	6 351.640 15	0.070 97	0.11	–0.004 33 (8)	0.118	1.1
R06e	6 353.103 13	0.068 94	0.19	–0.004 81 (12)	0.123	1.0
R08e	6 354.536 00	0.066 77	0.10	–0.004 70 (6)	0.124	1.0
R10e	6 355.938 80	0.065 36	0.09	–0.004 95 (6)	0.129	1.0
R12e	6 357.311 57	0.063 65	0.09	–0.005 33 (5)	0.127	1.0
R14e	6 358.654 38	0.062 02	0.11	–0.005 57 (6)	0.126	1.0
R16e	6 359.967 29	0.060 70	0.10	–0.006 00 (5)	0.110	1.3
R18e	6 361.250 40	0.059 74	0.10	–0.006 26 (5)	0.115	1.2
R20e	6 362.503 79	0.058 23	0.10	–0.006 31 (5)	0.109	1.4
R22e	6 363.727 61	0.057 18	0.12	–0.006 82 (7)	0.109	1.4
R24e	6 364.921 97	0.056 16	0.11	–0.006 94 (6)	0.102	1.6
R26e	6 366.087 03	0.055 31	0.11	–0.007 01 (6)	0.106	1.5
R28e	6 367.222 94	0.054 54	0.13	–0.007 22 (7)	0.104	1.6
R30e	6 368.329 89	0.053 70	0.11	–0.007 27 (6)	0.093	1.8
R32e	6 369.408 07	0.053 08	0.13	–0.007 89 (7)	0.090	1.9
R34e	6 370.457 70	0.052 69	0.13	–0.008 17 (8)	0.084	2.3
R36e	6 371.478 99	0.052 65	0.25	–0.008 10 (12)	0.117	1.5
R38e	6 372.472 21	0.051 14	0.18	–0.007 85 (11)	0.083	2.6
R40e	6 373.437 62	0.051 37	0.19	–0.008 53 (12)	0.111	1.5
R42e	6 374.375 49	0.050 88	0.22	–0.008 53 (10)	0.1	
R44e	6 375.286 14	0.049 96	0.28	–0.009 20 (13)	0.1	
R46e	6 376.169 89	0.049 86	0.52	–0.009 28 (24)	0.1	
R48e	6 377.027 07	0.048 91	0.49	–0.009 78 (23)	0.1	
R50e	6 377.858 06	0.048 15	0.64	–0.010 02 (30)	0.1	

Table 2 (*concluded*).

Line	Position[a]	b_L^0(Ar)[b]	Unc. (%)	δ^0(Ar)[c] unc.	SD[d]	Unc. (%)
R52e	6 378.663 24	0.048 65	1.15	–0.011 38 (54)	0.1	
R54e	6 379.443 02	0.047 72	1.30	–0.009 58 (60)	0.1	
R56e	6 380.197 83	0.042 49	3.22	–0.010 09 (133)	0.1	
R58e	6 380.928 12	0.049 67	3.26	–0.009 64 (157)	0.1	

[a]Zero pressure line center positions are in cm^{-1}. While the position values were adjusted during the present study, to the accuracy given here they are the same as in [4]. See text for details.

[b]The measured Ar-broadened half-width coefficients are in cm^{-1}/atm at 296 K.

[c]The measured Ar-induced pressure-shift coefficients are in cm^{-1}/atm at the temperature of the spectra (~294 K; see Table 1).

[d]Speed-dependence (SD) parameter (unitless).

The multispectrum retrieval constrained the line positions and line intensities of the fitted bands to well-known quantum mechanical expressions, so that spectroscopic parameters such as the rovibrational constants (G, B, D, H,...) and intensities (band intensities and Herman–Wallis factors) are determined directly from the whole band analysis rather than determining individual line positions and line intensities, from which the various constants are determined [34]. In contrast, the multispectrum algorithm adjusted the half-width and the pressure-shift coefficient for each measured transition individually in the least-squares fits. In the present study, we used the same set of self-broadened spectra used in [4, 5] to ensure the same level of accuracy for the retrieved Ar-broadened half-widths, pressure shifts, and line mixing coefficients. Line positions, intensities, self-broadened half-width, self-shift, and the off-diagonal relaxation matrix element coefficients for self-line mixing were fixed to values derived from the previous analyses [4, 5]. The parameters floated in the present study are the Ar-broadened half-width and Ar pressure-induced shift, the off-diagonal relaxation matrix element coefficients due to Ar-broadening for each measured line (or between a pair of lines for line mixing) in the 30012←00001 and 30013←00001 bands. We have used a single speed dependence parameter for each line in the multispectrum fit; thus, this parameter includes concentration weighted contributions from both CO_2 and Ar.

The widely used convenient, approximate expressions, used for retrieving the pressure-broadened half-width and pressure-induced shift coefficients are given below,

$$b_L(p,T) = p\left[b_L^0(\mathrm{Ar})(p_0,T_0)(1-\chi)\left(\frac{T_0}{T}\right)^{n1} + b_L^0(\mathrm{self})(p_0,T_0)\chi\left(\frac{T_0}{T}\right)^{n2}\right] \quad (1)$$

$$\nu = \nu_0 + p[\delta^0(\mathrm{Ar})(1-\chi) + \delta^0(\mathrm{self})\chi] \quad (2)$$

$$\delta^0(T) = \delta^0(T_0) + \delta'(T - T_0) \quad (3)$$

In (1)–(3), the reference pressure p_0 = 1 atm, the temperature T_0 = 296 K, b_L^0 and δ^0 represent the Lorentz pressure-broadened half-width (in cm^{-1}/atm at 296 K) and pressure-induced shift coefficients (in cm^{-1}/atm at 294 K). b_L (p, T) is the Lorentz half-width (in cm^{-1}) of the spectral line at pressure p and temperature T. b_L^0(Gas)(p_0, T_0) is the Lorentz half-width coefficient of the line at the reference pressure p_0 (1 atm) and temperature T_0 (296 K) of the broadening gas (either Ar or CO_2 in the present case), and χ is the ratio of the partial pressure of CO_2 to the total sample pressure in the cell.

The off diagonal relaxation matrix elements on one side of the diagonal are found from the coefficients provided. The other side is found from detailed balance for the two states with J and J + 2 for rotational quantum numbers,

$$W_{ji} = W_{ij}\frac{\rho(J+2)\times 2\times(J+3)}{\rho(J)\times 2\times(J+1)} \quad (4)$$

Here $\rho(J)$ is the population of molecules in the state with rotational quantum number J, as calculated from the Boltzman distribution and 2 × (J + 1) is the statistical weight of the same state. The relaxation matrix formulation for the calculation of line mixing is used for several reasons. The first is that it can be converted to the equivalent Rosenkranz formulation quite easily by the methods of refs. 33 and 34. but the inverse operation is either difficult (sometimes when the number of nonzero off-diagonal matrix elements determined is less than the number of lines mixing) or nonunique. Furthermore, the Rosenkranz formulation is only an approximation that breaks down at higher pressures where the separation of the lines is no longer much larger than the Lorentz width. The relaxation matrix elements also allow for the combination of mixing from simultaneous broadening by more than one gas. These elements also have physical meaning that allows them to be extended to other temperatures without measurement at every temperature. The Rosenkranz approximation can also lead to slightly different definitions of intensity, pressure shift, and zero-pressure position for different broadening gases, temperatures, and pressures.

The present analysis was performed for the P62–R58 transitions in the 30012←00001 band, P62–R60 transitions in the 30013←00001 band, and for P45–R46 in the 31112←01101 and 31113←01101 bands. For weak transitions outside these ranges, Lorentz self-broadened half-width coefficients were held fixed to HITRAN values [35, 36]. The Ar-broadened half-width coefficients for unmeasured transitions (transitions beyond our highest measured J'') were fixed to our present values determined at the highest J'' value. Both

Table 3. Ar-broadened half-width and pressure-induced shift coefficients and speed dependence in the 30013←00001 band of $^{16}O^{12}C^{16}O$.

Line	Position[a]	b_L^0(Ar)[b]	Unc. (%)	δ^0(Ar)[c] unc.	SD[d]	Unc. (%)
P62e	6 165.898 26	0.052 90	5.12	–0.014 04 (264)	0.1	
P60e	6 168.353 90	0.049 10	3.63	–0.016 66 (173)	0.1	
P58e	6 170.777 30	0.046 18	2.19	–0.008 80 (99)	0.1	
P56e	6 173.168 65	0.047 46	1.50	–0.008 21 (69)	0.1	
P54e	6 175.528 18	0.047 87	1.04	–0.009 33 (49)	0.1	
P52e	6 177.856 09	0.049 05	0.75	–0.008 27 (35)	0.1	
P50e	6 180.152 60	0.049 54	0.61	–0.009 64 (29)	0.1	
P48e	6 182.417 93	0.050 27	0.40	–0.008 89 (19)	0.1	
P46e	6 184.652 30	0.050 04	0.48	–0.009 73 (23)	0.062	6.0
P44e	6 186.855 91	0.050 85	0.26	–0.008 50 (11)	0.098	2.2
P42e	6 189.029 00	0.051 58	0.21	–0.008 53 (9)	0.108	1.7
P40e	6 191.171 76	0.051 93	0.17	–0.008 92 (11)	0.087	2.3
P38e	6 193.284 40	0.052 00	0.15	–0.008 44 (9)	0.094	1.9
P36e	6 195.367 14	0.053 25	0.13	–0.008 34 (8)	0.108	1.5
P34e	6 197.420 14	0.053 40	0.11	–0.008 27 (7)	0.111	1.4
P32e	6 199.443 62	0.054 13	0.11	–0.008 11 (6)	0.109	1.4
P30e	6 201.437 74	0.054 76	0.13	–0.008 24 (7)	0.107	1.5
P28e	6 203.402 68	0.055 64	0.11	–0.008 05 (5)	0.113	1.3
P26e	6 205.338 59	0.056 12	0.11	–0.007 98 (5)	0.107	1.4
P24e	6 207.245 63	0.057 55	0.12	–0.007 48 (7)	0.131	1.1
P22e	6 209.123 93	0.058 66	0.10	–0.007 57 (5)	0.131	1.0
P20e	6 210.973 63	0.059 64	0.10	–0.007 16 (5)	0.131	1.0
P18e	6 212.794 85	0.061 17	0.10	–0.007 21 (5)	0.141	0.9
P16e	6 214.587 68	0.062 45	0.10	–0.007 09 (5)	0.126	1.1
P14e	6 216.352 21	0.064 47	0.11	–0.006 89 (6)	0.151	0.8
P12e	6 218.088 53	0.065 34	0.09	–0.006 35 (5)	0.146	0.8
P10e	6 219.796 71	0.067 20	0.12	–0.006 57 (7)	0.145	0.8
P08e	6 221.476 78	0.068 90	0.10	–0.005 74 (6)	0.136	0.9
P06e	6 223.128 78	0.070 34	0.10	–0.005 43 (7)	0.134	0.9
P04e	6 224.752 75	0.072 91	0.12	–0.005 53 (10)	0.127	1.0
P02e	6 226.348 68	0.077 05	0.18	–0.003 88 (17)	0.117	1.2
R00e	6 228.689 98	0.081 26	0.30	–0.001 60 (31)	0.091	2.6
R02e	6 230.215 76	0.074 09	0.13	–0.003 79 (11)	0.127	1.0
R04e	6 231.713 42	0.071 17	0.10	–0.004 18 (8)	0.118	1.1
R06e	6 233.182 89	0.069 13	0.10	–0.004 48 (6)	0.141	0.8
R08e	6 234.624 10	0.067 25	0.09	–0.004 42 (6)	0.139	0.9
R10e	6 236.036 97	0.065 35	0.09	–0.004 83 (5)	0.139	0.9
R12e	6 237.421 40	0.063 92	0.09	–0.005 30 (5)	0.136	0.9
R14e	6 238.777 27	0.062 17	0.10	–0.005 42 (5)	0.137	0.9
R16e	6 240.104 44	0.060 81	0.10	–0.005 85 (5)	0.130	1.0
R18e	6 241.402 78	0.059 65	0.10	–0.006 24 (5)	0.121	1.2
R20e	6 242.672 14	0.058 06	0.09	–0.006 25 (5)	0.113	1.3
R22e	6 243.912 34	0.057 22	0.10	–0.006 70 (5)	0.124	1.1
R24e	6 245.123 21	0.056 04	0.11	–0.006 73 (5)	0.105	1.5
R26e	6 246.304 55	0.055 25	0.10	–0.007 09 (5)	0.105	1.6
R28e	6 247.456 16	0.054 26	0.11	–0.007 44 (5)	0.094	1.8
R30e	6 248.577 83	0.053 70	0.11	–0.007 46 (6)	0.100	1.7
R32e	6 249.669 34	0.053 20	0.11	–0.007 47 (6)	0.091	2.0
R34e	6 250.730 46	0.052 43	0.11	–0.007 94 (7)	0.072	2.9
R36e	6 251.760 95	0.052 21	0.13	–0.007 93 (8)	0.098	1.8
R38e	6 252.760 57	0.051 52	0.16	–0.008 19 (9)	0.075	2.9
R40e	6 253.729 06	0.050 68	0.18	–0.008 24 (7)	0.077	2.8
R42e	6 254.666 16	0.050 63	0.20	–0.008 51 (9)	0.083	2.6
R44e	6 255.571 62	0.050 23	0.24	–0.009 01 (11)	0.096	2.3
R46e	6 256.445 16	0.049 61	0.30	–0.009 83 (14)	0.103	2.4
R48e	6 257.286 53	0.049 29	0.39	–0.009 30 (18)	0.1	

Table 3 (*concluded*).

Line	Position[a]	$b_L{}^0$(Ar)[b]	Unc. (%)	δ^0(Ar)[c] unc.	SD[d]	Unc. (%)
R50e	6 258.095 45	0.048 16	0.52	–0.008 37 (24)	0.1	
R52e	6 258.871 66	0.047 65	0.71	–0.010 03 (33)	0.1	
R54e	6 259.614 88	0.047 24	1.01	–0.008 80 (46)	0.1	
R56e	6 260.324 86	0.047 80	1.44	–0.009 10 (69)	0.1	
R58e	6 261.001 32	0.045 10	2.11	–0.009 85 (94)	0.1	
R60e	6 261.644 02	0.047 55	3.18	–0.009 99 (150)	0.1	

[a]Zero-pressure line center positions are in cm^{-1}. While the position values were adjusted during the present study, to the accuracy given here they are the same as in [5]. See text for details.

[b]The measured Ar-broadened half-width coefficients are in cm^{-1}/atm at 296 K.

[c]The measured Ar-induced pressure-shift coefficients are in cm^{-1}/atm at the temperature of the spectra ($\sim$294 K; see Table 1).

[d]Speed-dependence (SD) parameter (unitless).

self- and Ar-induced pressure-shift coefficients for unfitted transitions were fixed to a default value of –0.005 cm^{-1}/atm, a value that is comparable to the majority of the measured pressure-induced shift coefficients in this wavenumber region [4, 5]. The temperature dependence exponents of the Ar-broadened half-width (n_1 in (1)) and the self-broadened half-width coefficient (n_2 in (1)) were assumed equal to the n_1 values in HITRAN [35, 36], which range between 0.69 and 0.78 depending upon the J'' value of the transition. Since the gas temperatures in the present data were close to 296 K, assuming identical temperature exponents for both and self- and Ar-broadening introduced errors no larger than 0.05% in the retrieved broadening coefficients. The temperature dependences of all self- and Ar-shift coefficients were set to zero. This assumption also introduced no noticeable residuals in the least-squares fits.

4. Results and discussion

4.1. Ar-broadened half-width and pressure-shift coefficients

The final multispectrum fit to all 21 spectra for the 6280 to 6395 cm^{-1} interval covering 30012←00001 band is plotted in Fig. 1. Weaker absorption features from the 31112← 01101 hot band and other interfering hot band and isotopologue lines also appear in the fitted region. Figure 1*a* shows the 21 observed spectra. Figure 1*b* shows the weighted fit residuals from all 21 spectra using a speed-dependent Voigt profile and line mixing calculated via the relaxation matrix [33, 34]. Figure 1*c* shows only the weighted fit residuals from the 6 Ar-broadened spectra (copied from Fig. 1*b* for purpose of illustration). Panels *b* and *c* of Fig. 1 demonstrate that the signal-to-noise based weighting scheme produces consistently high quality fits in all spectra.

The results from the multispectrum least-squares fits are listed in Tables 2–6. The results for the 30012←00001 band are given in Table 2. The rovibrational (G, B, D, H,. . .) and intensity (S_v, a_1, a_2) parameters were constrained to the values reported in [4]. The self-broadened half-width and self-shift coefficients, as well as the self induced off-diagonal relaxation matrix elements were also fixed to the measured values from [4]. This procedure ensures maximum accuracy in the Ar-broadened half-width and pressure shift coefficients as well as consistency with our previous work. To confirm the robustness of the Ar-broadened multispectrum fit, the rovibrational (G, B, D, H,. . .) and intensity (S_v, a_1, a_2) parameters were floated in the final fit to determine how much variation this introduced into the results. As expected, the final parameter values determined in the present study were well within the uncertainty ranges for all of the parameters reported in [4]. The truncated positions listed in Table 2 are presented for ease in identifying different transitions.

The Lorentz Ar pressure-broadened half-width coefficients b_L^0 (Ar) (in cm^{-1}/atm at 296 K), the Ar pressure-induced shift coefficients δ^0(Ar) (in cm^{-1}/atm at $\sim$294 K), and the values determined from the least-squares fit for speed dependence parameters (unitless) for self- and Ar-broadening are also listed in Table 2. Since no temperature dependence was assumed for the Ar pressure-induced shift coefficients δ^0(Ar), the listed values correspond to the temperature of the data ($\sim$294 K). For the Ar pressure-broadened half-width coefficients b_L^0 (Ar), a default value of 0.75 was used as the temperature dependence exponent for all transitions, and hence the values listed correspond to a reference temperature of 296 K, as assumed in HITRAN database [35, 36]. The uncertainties in Ar-broadened half-width coefficients and speed dependence parameters are given as percentages. The measured uncertainties in the Ar pressure-shift coefficients listed in parentheses are in units of the least significant digits reported. The uncertainty represents one standard deviation in the measured quantity in all instances.

Table 3 presents the results for the 30013←00001 band. As with the 30012←00001 multispectrum fit, the line positions, intensities, self-broadened half-widths, and self-induced shift coefficients for bands studied in [5] were held fixed during the analysis of Ar-broadened half-width and pressure-shift coefficients for the 30013←00001 band. The test fit floated the rovibrational (G, B, D, H,. . .) and intensity (S_v, a_1, a_2) parameters and these were determined within the experimental uncertainties reported in [5].

Ar-broadened half-width and Ar-induced pressure-shift coefficients for the 31112←01101 and the 31113←01101 hot bands were also measured because of the fairly large volume mixing ratios of CO_2 in the Ar-broadened spectra used in this work and compared with the air-broadened spectra analyzed in the previous investigations [4, 5]. The measurements obtained for the hot band transitions are less extensive and less accurate than the values obtained for the

Table 4. Ar-broadened half-width and pressure-shift coefficients in the 31112←01101 band of $^{16}O^{12}C^{16}O$.

Line	Position[a]	$b_L^0(Ar)$[b]	Unc. (%)	$\delta^0(Ar)$[c] unc.
P45e	6 313.548 92	0.041 90	6.99	
P43e	6 315.771 07	0.047 34	5.39	–0.006 35 (256)
P41e	6 317.964 14	0.049 90	4.17	–0.004 75 (208)
P39e	6 320.127 97	0.054 59	4.07	–0.012 13 (222)
P37e	6 322.262 38	0.048 72	3.63	–0.009 55 (178)
P35e	6 324.367 23	0.059 25	2.16	–0.007 36 (128)
P33e	6 326.442 36	0.053 08	1.70	–0.013 15 (90)
P31e	6 328.487 64	0.052 28	1.43	–0.008 67 (75)
P29e	6 330.502 94	0.053 99	1.28	–0.009 36 (68)
P27e	6 332.488 13	0.056 93	1.32	–0.008 89 (74)
P25e	6 334.443 10	0.044 73	4.29	–0.014 62 (187)
P23e	6 336.367 75	0.056 75	1.21	–0.005 30 (70)
P21e	6 338.261 97	0.059 30	0.86	–0.006 80 (51)
P19e	6 340.125 66	0.060 24	0.78	–0.007 26 (46)
P17e	6 341.958 75	0.062 81	0.75	–0.005 88 (47)
P15e	6 343.761 15	0.061 94	0.74	–0.005 12 (46)
P13e	6 345.532 79	0.062 50	0.77	–0.006 68 (47)
P11e	6 347.273 61	0.064 38	0.82	–0.005 38 (53)
P09e	6 348.983 53	0.068 36	0.95	–0.005 98 (65)
P05e	6 352.310 49	0.068 15	1.58	–0.004 10 (107)
P03e	6 353.927 44	0.078 31	2.83	–0.011 28 (222)
R01e	6 357.833 81	0.066 11	4.87	–0.005 16 (322)
R03e	6 359.341 89	0.071 83	2.02	–0.004 90 (144)
R05e	6 360.818 82	0.071 72	1.37	–0.004 42 (98)
R07e	6 362.264 59	0.070 86	1.16	–0.006 37 (82)
R09e	6 363.679 19	0.067 47	2.43	–0.001 03 (163)
R11e	6 365.062 62	0.066 45	1.02	–0.005 97 (68)
R13e	6 366.414 91	0.063 44	0.76	–0.004 20 (47)
R15e	6 367.736 06	0.060 43	0.71	–0.006 12 (43)
R17e	6 369.026 09	0.059 26	0.73	–0.004 95 (42)
R19e	6 370.285 03	0.059 45	0.81	–0.006 40 (47)
R21e	6 371.512 91	0.055 73	1.81	–0.007 81 (103)
R23e	6 372.709 79	0.055 49	0.88	–0.007 13 (48)
R25e	6 373.875 70	0.057 32	1.24	–0.006 54 (70)
R27e	6 375.010 70	0.051 22	1.62	–0.005 11 (83)
R29e	6 376.114 86	0.052 18	1.67	–0.007 90 (87)
R31e	6 377.188 25	0.052 57	1.41	–0.006 44 (74)
R33e	6 378.230 94	0.052 62	1.65	–0.009 77 (87)
R35e	6 379.243 01	0.051 10	2.02	–0.009 73 (103)
R37e	6 380.224 58	0.052 78	4.41	–0.003 06 (231)
R39e	6 381.175 73	0.051 73	3.21	–0.007 23 (165)
R45e	6 383.847 88	0.041 78	7.10	–0.015 03 (297)
P46f	6 313.948 49	0.050 48	8.60	
P44f	6 316.050 49	0.043 59	6.15	–0.011 68 (269)
P42f	6 318.129 89	0.051 59	4.87	–0.011 71 (251)
P40f	6 320.186 50	0.050 83	4.58	–0.008 97 (233)
P38f	6 322.220 11	0.054 32	4.20	–0.013 57 (228)
P36f	6 324.230 54	0.053 06	2.36	–0.005 88 (125)
P34f	6 326.217 60	0.054 79	1.88	–0.007 72 (103)
P32f	6 328.181 14	0.054 24	1.55	–0.004 57 (83)
P30f	6 330.120 98	0.057 01	1.33	–0.007 55 (75)
P28f	6 332.037 00	0.053 99	1.13	–0.008 78 (61)
P26f	6 333.929 03	0.057 35	1.01	–0.008 69 (58)
P24f	6 335.796 95	0.056 53	0.92	–0.007 33 (52)
P22f	6 337.640 64	0.058 14	0.86	–0.008 14 (50)
P20f	6 339.459 98	0.060 77	0.86	–0.008 85 (52)
P18f	6 341.254 86	0.060 43	0.96	–0.007 10 (59)
P16f	6 343.025 19	0.058 26	2.47	–0.002 88 (136)
P14f	6 344.770 87	0.064 22	1.09	–0.007 75 (75)
P12f	6 346.491 82	0.064 24	0.84	–0.007 74 (53)
P10f	6 348.187 97	0.067 18	0.88	–0.006 99 (59)
P08f	6 349.859 25	0.071 30	1.08	–0.007 00 (76)
P06f	6 351.505 60	0.074 89	1.71	–0.001 62 (132)
P04f	6 353.126 97	0.067 64	7.92	0.000 42 (509)
P02f	6 354.723 31	0.072 73	6.00	–0.007 77 (436)
R02f	6 358.604 48	0.065 30	7.61	–0.009 40 (498)
R04f	6 360.113 01	0.073 02	2.15	0.001 01 (159)
R06f	6 361.596 42	0.068 32	1.20	–0.002 13 (82)
R08f	6 363.054 70	0.066 50	0.95	–0.004 54 (63)
R10f	6 364.487 87	0.064 49	0.84	–0.003 44 (53)
R12f	6 365.895 93	0.063 65	0.86	–0.005 03 (54)
R14f	6 367.278 91	0.064 39	1.44	–0.004 83 (97)
R16f	6 368.636 84	0.062 16	0.74	–0.004 51 (45)
R18f	6 369.969 75	0.060 41	0.73	–0.007 25 (43)
R20f	6 371.277 70	0.058 54	0.80	–0.004 55 (46)
R22f	6 372.560 74	0.056 41	1.03	–0.005 63 (60)
R24f	6 373.818 93	0.053 27	1.16	–0.004 87 (61)
R26f	6 375.052 34	0.056 78	1.57	–0.007 65 (88)
R28f	6 376.261 06	0.053 81	1.28	–0.009 11 (68)
R30f	6 377.445 17	0.050 71	1.26	–0.010 38 (64)
R32f	6 378.604 77	0.056 47	2.00	–0.008 60 (112)
R34f	6 379.739 96	0.055 31	1.86	–0.009 11 (102)
R36f	6 380.850 87	0.058 10	2.65	–0.008 87 (154)
R38f	6 381.937 61	0.049 03	2.86	–0.009 82 (140)
R42f	6 384.039 16	0.048 86	4.72	–0.010 88 (232)
R44f	6 385.054 27	0.037 73	6.07	–0.017 06 (230)
R46f	6 386.045 81	0.043 13	8.37	

[a]Zero pressure line center positions are in cm^{-1}. The position values are the same as in [4] and were held fixed during the present study.

[b]The measured Ar-broadened half-width coefficients are in cm^{-1}/atm at 296 K.

[c]The measured Ar-induced pressure-shift coefficients are in cm^{-1}/atm at the temperature of the spectra (∼294 K; see Table 1).

stronger 30012←00001 and the 30013←00001 bands. The results obtained for the 31112←01101 and the 31113←01101 bands are listed in Tables 4 and 5, respectively. Because the transitions in these hot bands were weak, line mixing and speed dependence were neither determinable nor required to fit the data for these bands to the experimental noise level (see Fig. 1).

The measured Ar-broadened half-width coefficients for the 30012←00001 and the 30013←00001 bands and the associated 31112←01101 and 31113←01101 hot bands are plotted as a function of m ($m = -J''$ and $J'' + 1$, for the P- and R-branch transitions) in Fig. 2. The Q-branch transitions in the 31112←01101 and the 31113←01101 were weak, and neither broadening nor shift coefficients were measured for those transitions. The parameters for 30012←00001 and 30013←00001 bands are plotted in panel (Fig. 2*a*), and the corresponding values for the 31112←01101 and the 31113←01101 bands in panel (Fig. 2*b*). The Ar-broadened half-width coefficients of Valero and Suarez [11], Suarez

Table 5. Ar-broadened half-width and pressure-induced shift coefficients in the 31113←01101 band of $^{16}O^{12}C^{16}O$.

Line	Position[a]	b_L^0(Ar)[b]	Unc. (%)	δ^0(Ar)[c]
P45e	6 153.693 42	0.047 15	6.26	–0.012 30 (296)
P43e	6 155.900 06	0.051 17	4.81	–0.003 40 (247)
P41e	6 158.076 76	0.053 09	3.72	–0.013 21 (199)
P39e	6 160.223 62	0.049 75	3.05	–0.008 93 (152)
P35e	6 164.428 19	0.057 19	2.03	–0.008 00 (116)
P33e	6 166.486 03	0.054 21	1.53	–0.007 89 (83)
P31e	6 168.514 30	0.056 34	1.31	–0.007 20 (74)
P29e	6 170.513 04	0.054 60	1.09	–0.008 48 (60)
P27e	6 172.482 27	0.056 20	0.96	–0.007 21 (54)
P25e	6 174.421 99	0.056 99	0.86	–0.007 99 (49)
P23e	6 176.332 22	0.057 89	0.80	–0.007 34 (45)
P21e	6 178.212 96	0.058 31	0.74	–0.006 36 (42)
P19e	6 180.064 19	0.058 24	0.79	–0.007 10 (46)
P17e	6 181.885 90	0.059 86	0.68	–0.006 68 (41)
P15e	6 183.678 09	0.062 73	0.70	–0.006 95 (43)
P13e	6 185.440 72	0.064 50	0.73	–0.006 15 (46)
P11e	6 187.173 79	0.066 76	0.79	–0.005 23 (52)
P09e	6 188.877 26	0.070 41	0.95	–0.005 78 (67)
P07e	6 190.551 11	0.069 97	1.09	–0.005 74 (76)
P05e	6 192.195 32	0.070 79	1.48	–0.008 67 (104)
R05e	6 200.707 42	0.069 63	1.22	–0.006 69 (85)
R07e	6 202.158 32	0.068 23	0.95	–0.004 24 (64)
R09e	6 203.579 37	0.068 99	0.93	–0.004 39 (63)
R11e	6 204.970 55	0.064 40	0.75	–0.003 24 (47)
R13e	6 206.331 84	0.063 30	0.68	–0.006 10 (42)
R15e	6 207.663 21	0.061 67	0.66	–0.004 52 (41)
R17e	6 208.964 61	0.061 55	0.81	–0.005 11 (50)
R19e	6 210.236 02	0.058 89	0.68	–0.007 08 (39)
R21e	6 211.477 39	0.057 94	0.72	–0.006 81 (41)
R23e	6 212.688 68	0.054 46	1.23	–0.007 41 (68)
R25e	6 213.869 84	0.055 54	1.29	–0.008 18 (72)
R27e	6 215.020 81	0.055 22	1.26	–0.005 99 (70)
R29e	6 216.141 53	0.056 45	1.28	–0.006 63 (72)
R31e	6 217.231 92	0.053 60	1.25	–0.005 93 (67)
R33e	6 218.291 90	0.054 80	1.73	–0.009 97 (94)
R35e	6 219.321 38	0.053 90	1.81	–0.006 40 (98)
R37e	6 220.320 23	0.052 30	2.22	–0.006 80 (116)
R41e	6 222.225 57	0.050 62	3.56	–0.006 66 (181)
R45e	6 224.006 72	0.053 37	6.26	
R47e	6 224.850 25	0.053 05	11.12	
P48f	6 152.010 23	0.042 35	9.66	–0.010 57 (410)
P46f	6 154.124 41	0.043 53	7.28	–0.005 54 (318)
P44f	6 156.213 97	0.049 59	5.51	–0.007 41 (274)
P42f	6 158.279 10	0.041 96	4.22	–0.011 33 (177)
P40f	6 160.319 94	0.046 94	3.43	–0.012 79 (161)
P36f	6 164.329 38	0.049 68	2.19	–0.004 47 (109)
P34f	6 166.298 22	0.054 64	1.70	–0.005 81 (93)
P32f	6 168.243 28	0.053 31	1.48	–0.005 84 (79)
P30f	6 170.164 66	0.055 94	1.19	–0.008 16 (67)
P28f	6 172.062 43	0.055 16	1.03	–0.006 22 (56)
P26f	6 173.936 66	0.053 67	0.91	–0.004 57 (48)
P24f	6 175.787 41	0.057 27	0.82	–0.006 07 (47)
P22f	6 177.614 74	0.057 00	0.75	–0.007 34 (43)
P20f	6 179.418 68	0.059 56	0.72	–0.007 74 (42)
P18f	6 181.199 27	0.061 35	0.70	–0.006 29 (42)
P16f	6 182.956 53	0.061 69	0.70	–0.006 98 (42)

Table 5 (*concluded*).

Line	Position[a]	b_L^0(Ar)[b]	Unc. (%)	δ^0(Ar)[c]
P14f	6 184.690 49	0.060 01	1.15	–0.005 12 (67)
P12f	6 186.401 16	0.063 27	0.74	–0.004 49 (47)
P10f	6 188.088 53	0.066 39	0.83	–0.005 93 (55)
P08f	6 189.752 63	0.068 05	0.97	–0.008 18 (66)
P06f	6 191.393 43	0.071 82	1.31	–0.011 34 (92)
P04f	6 193.010 93	0.074 15	1.93	–0.008 15 (141)
R04f	6 200.000 85	0.070 16	1.45	–0.005 68 (102)
R06f	6 201.489 80	0.066 56	2.05	–0.004 79 (145)
R08f	6 202.955 27	0.067 23	0.88	–0.005 60 (58)
R10f	6 204.397 21	0.064 62	0.76	–0.003 60 (48)
R12f	6 205.815 55	0.062 30	0.70	–0.005 55 (43)
R16f	6 208.581 25	0.061 54	0.67	–0.006 58 (40)
R18f	6 209.928 45	0.058 77	0.66	–0.005 63 (38)
R20f	6 211.251 80	0.058 33	0.73	–0.004 68 (43)
R22f	6 212.551 20	0.057 57	0.83	–0.006 47 (48)
R24f	6 213.826 56	0.056 73	1.26	–0.005 98 (71)
R26f	6 215.077 77	0.055 77	1.18	–0.007 41 (66)
R28f	6 216.304 73	0.048 93	2.84	–0.004 95 (135)
R30f	6 217.507 31	0.054 09	1.16	–0.007 79 (62)
R32f	6 218.685 39	0.052 62	1.37	–0.006 49 (71)
R34f	6 219.838 81	0.050 56	4.41	–0.001 71 (217)
R36f	6 220.967 42	0.054 48	2.02	–0.009 37 (110)
R38f	6 222.071 06	0.049 66	2.50	–0.011 52 (124)
R42f	6 224.202 65	0.054 12	4.10	–0.007 14 (222)
R44f	6 225.230 19	0.053 17	5.44	–0.011 03 (291)
R46f	6 226.231 93	0.048 84	8.39	

[a]Zero-pressure line center positions are in cm^{-1}. The position values are the same as in [5] and were held fixed during the present study.
[b]The measured Ar-broadened half-width coefficients are in cm^{-1}/atm at 296 K.
[c]The measured Ar-induced pressure-shift coefficients are in cm^{-1}/atm at the temperature of the spectra (~294 K; see Table 1).

and Valero [12], Nakamichi et al. [30], Thibault et al. [13], and Li et al. [32] are also plotted in Fig. 2*a* for comparison. The agreement between our results and those of Valero and Suarez [11] is good, especially for transitions with $10 \le m \le 30$, despite the significant differences in uncertainties, instrumentation, resolution, data analysis methods, etc. The results reported by Nakamichi et al. [30] for transitions in the 30013←00001 compare well with present measurements, except for R0. Although there is good agreement in the R-branch measurements between present study and the measurements of $3\nu_3$ band by Thibault et al. [13], there are some differences seen in the results for the P-branch transitions. The values of Li et al. [32] for R0 to R20 average slightly higher than the present results. As can be expected, the uncertainties in the Ar-broadened half-width coefficients for the 31112←01101 and the 31113←01101 bands (Fig. 2*b*) are larger than those for the 30012←00001 and the 30012←00001 bands.

The measured Ar-broadened half-width coefficients for lines in the 30012←00001 and the 30013←00001 bands are compared with previously measured self- and air-broadening coefficients [4, 5] and the half-width coefficients for all three broadening gases are plotted as a function of m in Fig. 3. The results for the 30012←00001 band are plotted

Table 6. Off-diagonal relaxation matrix element coefficients (W_{ij}) for 30012← 00001 and 30013–00001 bands of $^{16}O\ ^{12}C^{16}O$ for CO_2–Ar broadening.

Line mixing between	Self-$W_{ij}^{CO_2-CO_2}$(296 K) 30012←00001	Air-$W_{ij}^{CO_2-air}$(296 K) 30012←00001	Argon-$W_{ij}^{CO_2-Ar}$(296 K) 30012←00001	Argon-$W_{ij}^{CO_2-Ar}$(296 K) 30013←00001
P2 to P4	0.0076 (1)	0.0087 (8)	0.0047(6)	0.0034(6)
P4 to P6	0.0137 (1)	0.0117 (8)	0.0035(6)	0.0078(6)
P6 to P8	0.0175 (2)	0.0163 (8)	0.0072(6)	0.0101(6)
P8 to P10	0.0207 (2)	0.0186 (8)	0.0113(6)	0.0135(6)
P10 to P12	0.0227 (2)	0.0205 (8)	0.0129(6)	0.0136(6)
P12 to P14	0.0248 (2)	0.0214 (8)	0.0145(6)	0.0168(6)
P14 to P16	0.0266 (2)	0.0241 (9)	0.0160(7)	0.0180(7)
P16 to P18	0.0274 (2)	0.0228 (9)	0.0167(7)	0.0190(7)
P18 to P20	0.0283 (2)	0.0241 (10)	0.0184(7)	0.0183(7)
P20 to P22	0.0282 (2)	0.0271 (10)	0.0178(8)	0.0186(8)
P22 to P24	0.0285 (2)	0.0253 (11)	0.0176(8)	0.0179(8)
P24 to P26	0.0279 (2)	0.0241 (12)	0.0169(9)	0.0179(9)
P26 to P28	0.0267 (3)	0.0219 (14)	0.0163(10)	0.0156(10)
P28 to P30	0.0256 (3)	0.0204 (15)	0.0170(11)	0.0141(11)
P30 to P32	0.0238 (3)	0.0159 (16)	0.0141(12)	0.0112(12)
P32 to P34	0.0213 (3)	0.0120 (17)	0.0137(12)	0.0103(13)
P34 to P36	0.0163 (3)	0.0087 (18)	0.0112(12)	0.0104(14)
P36 to P38	0.0131 (3)	0.0088 (16)	0.0125(11)	0.0089(15)
P38 to P40	0.0099 (3)	0.004 Fixed	0.004 Fixed	0.0087(13)
P40 to P42	0.0064 (3)	0.004 Fixed	0.004 Fixed	0.004 Fixed
P42 to P44	0.004 Fixed	0.004 Fixed	0.004 Fixed	0.004 Fixed
P44 to P46	0.004 Fixed	0.004 Fixed	0.004 Fixed	0.004 Fixed
P46 to P48	0.004 Fixed	0.004 Fixed	0.004 Fixed	0.004 Fixed
P48 to P50	0.004 Fixed	0.004 Fixed	0.004 Fixed	0.004 Fixed
R0 to R2	0.0048 (1)	0.0034 (6)	0.0012(4)	0.0007(4)
R2 to R4	0.0156 (1)	0.0112 (8)	0.0080(6)	0.0072(6)
R4 to R6	0.0215 (1)	0.0155 (8)	0.0117(6)	0.0093(6)
R6 to R8	0.0256 (2)	0.0201 (7)	0.0139(6)	0.0121(5)
R8 to R10	0.0288 (2)	0.0212 (7)	0.0148(5)	0.0127(5)
R10 to R12	0.0306 (2)	0.0213 (6)	0.0145(5)	0.0135(5)
R12 to R14	0.0320 (2)	0.0216 (6)	0.0149(5)	0.0145(5)
R14 to R16	0.0333 (2)	0.0223 (7)	0.0153(5)	0.0146(5)
R16 to R18	0.0338 (2)	0.0234 (7)	0.0159(5)	0.0148(5)
R18 to R20	0.0335 (2)	0.0233 (7)	0.0163(5)	0.0149(5)
R20 to R22	0.0328 (2)	0.0237 (7)	0.0156(6)	0.0147(5)
R22 to R24	0.0319 (2)	0.0232 (7)	0.0153(6)	0.0151(5)
R24 to R26	0.0310 (2)	0.0222 (8)	0.0147(6)	0.0142(5)
R26 to R28	0.0296 (2)	0.0222 (8)	0.0140(7)	0.0135(5)
R28 to R30	0.0288 (2)	0.0206 (9)	0.0135(7)	0.0138(5)
R30 to R32	0.0272 (3)	0.0191 (10)	0.0109(8)	0.0139(6)
R32 to R34	0.0257 (3)	0.0175 (10)	0.0113(8)	0.0115(6)
R34 to R36	0.0239 (3)	0.0165 (11)	0.0116(8)	0.0108(5)
R36 to R38	0.0211 (3)	0.0106 (11)	0.0098(7)	0.0096(5)
R38 to R40	0.0184 (3)	0.0078 (10)	0.0057(7)	0.004 Fixed
R40 to R42	0.0164 (4)	0.004 Fixed	0.004 Fixed	0.004 Fixed
R42 to R44	0.0130 (4)	0.004 Fixed	0.004 Fixed	0.004 Fixed
R44 to R46	0.0095 (4)	0.004 Fixed	0.004 Fixed	0.004 Fixed
R46 to R48	0.0070 (4)	0.004 Fixed	0.004 Fixed	0.004 Fixed
R48 to R50	0.0050 (4)	0.004 Fixed	0.004 Fixed	0.004 Fixed

Note: Units are cm^{-1}/atm near 296 K. The values given in parentheses represent one standard deviation uncertainties in the last quoted digits. The off-diagonal relaxation matrix element coefficients for self- and air-broadening (as examples) are listed only for the 30012←00001 band. The corresponding values for the 30013←00001 are available in ref. 5.

[a]

on the left-side panels and those for the 30013←00001 band on the right-side panels. Similar to previous studies [4, 5] the Ar-broadened half-width coefficients are fitted to the empirical functions given in Toth et al. [2, 3]. It is clear that for a given transition the Ar-broadened half-width coefficient (circles) is smaller than both the self- and air-

Fig. 2. Comparison of measured Ar-broadened half-width coefficients in 30012←00001 and 30013←00001; and in 31112←01101 and 31113←01101 bands using the same spectra and analysis technique. (*a*) Measured Ar-broadened half-width coefficients (cm^{-1}/atm at 296 K) of the 30012←00001 and 30013←00001 bands of $^{16}O^{12}C^{16}O$ plotted as a function of *m* ($m = -J''$ for P-branch lines and $J'' + 1$ for R-branch lines). CO_2–Ar half-width coefficients measured by several investigators for the same bands as in present study and also by Thibault et al. [13] for the $3\nu_3$ band are plotted for comparison. (*b*) Measured Ar-broadened half-width coefficients (cm^{-1}/atm at 296 K) of the 31112←01101 and 31113←01101 bands of $^{16}O^{12}C^{16}O$ plotted as a function of *m*. For clarity, transitions for the *e* and *f* species are plotted separately. Where error bars are not visible, the measured uncertainties are smaller than the size of the symbols used.

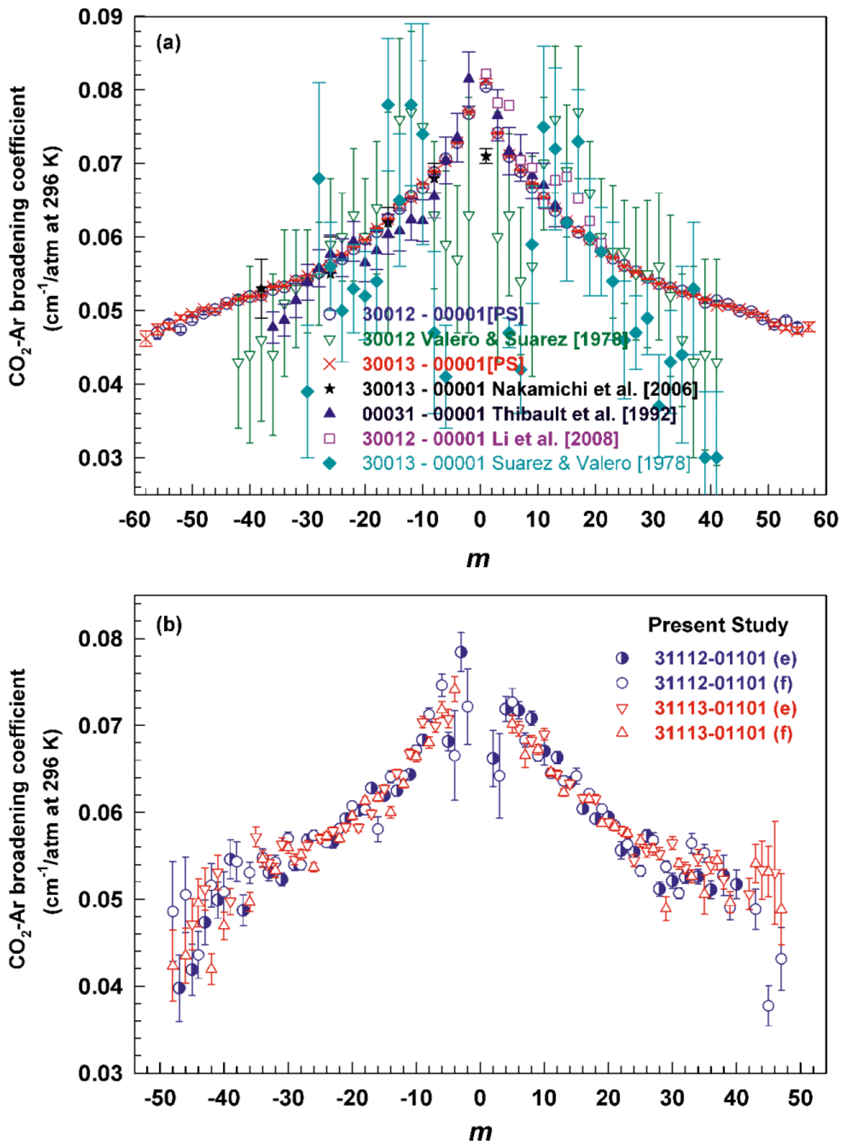

broadened half-width coefficients. The three curves (dashed, dash-dot-dash, and solid) passing through the corresponding measured points (Fig. 3, panels 3*a* and 3*d*) represent calculated self-, air- and Ar-broadened half-width coefficients, respectively.

The percentage differences between the measured and empirically calculated Ar-broadened half-width coefficients for the 30012←00001 and 30013←00001 bands are plotted as a function of *m* in Figs. 3*b* and 3*e*, respectively. The differences in both cases are within ±1.5%, except for a few high-*J* transitions where the weak absorptions are fitted with lower accuracy. The measured line-to-line variation is smooth to the 0.1% level, as seen in Figs. 3*a* and 3d and in values given in Tables 2 and 3. Since the measured half-width coefficients are not completely represented by the systematically different calculated values from the fitted curves, the parameters of the fit are not given and the measured values should be used instead. Closer examination of the residuals plotted in Figs. 3*b* and 3*e* indicates small systematic *m*-dependent differences. These residuals exceed the typical line-to-line variations seen in Figs. 3*a* and 3*d* and are similar in magnitude to the percentage differences previously observed for self- and air-broadened half-width coefficients (see Fig. 8 of [4] and Fig. 7 of [5]). However, the systematic differences in the percentage residuals between the P- and R-branch lines suggest that the measured half-width coefficients for P- and R-branch transitions differ for the same |*m*|. The mean and standard deviation of the ratios of P- to

Fig. 3. Comparison of measured self-, air-, and Ar-broadened half-width coefficients in 30012←00001 and 30013←00001 bands using the same spectra and analysis technique. The results for the 30012←00001 band are plotted on the left side panels (*a*)–(*c*) and those for the 30013←00001 bands on the right side panels (*d*)-(*f*). (*a*) Measured Ar-broadened half-width coefficients (cm^{-1}/atm at 296 K) of the 30012← 00001 band of $^{16}O^{12}C^{16}O$ are re-plotted as a function of *m*. The measured Ar-broadened half-width coefficients are fitted to the empirical expression given in [2, 3], and the calculated half-width coefficients are plotted by a solid curve. The self- and air-broadened half-width coefficients from our previous study [4] are also plotted for comparison purposes. (*b*) The percentage observed minus calculated residuals obtained for Ar-broadened half-width coefficients are plotted as a function of *m*. (*c*) The ratios of self- to Ar-broadened half-width coefficients are plotted as a function of *m*. The ratios of self- to air and air- to Ar-broadened half-width coefficients are also plotted for comparison. Similar results for the 30013←00001 band are displayed in (*d*)–(*f*). Where error bars are not visible the uncertainties are smaller than the size of the symbols used.

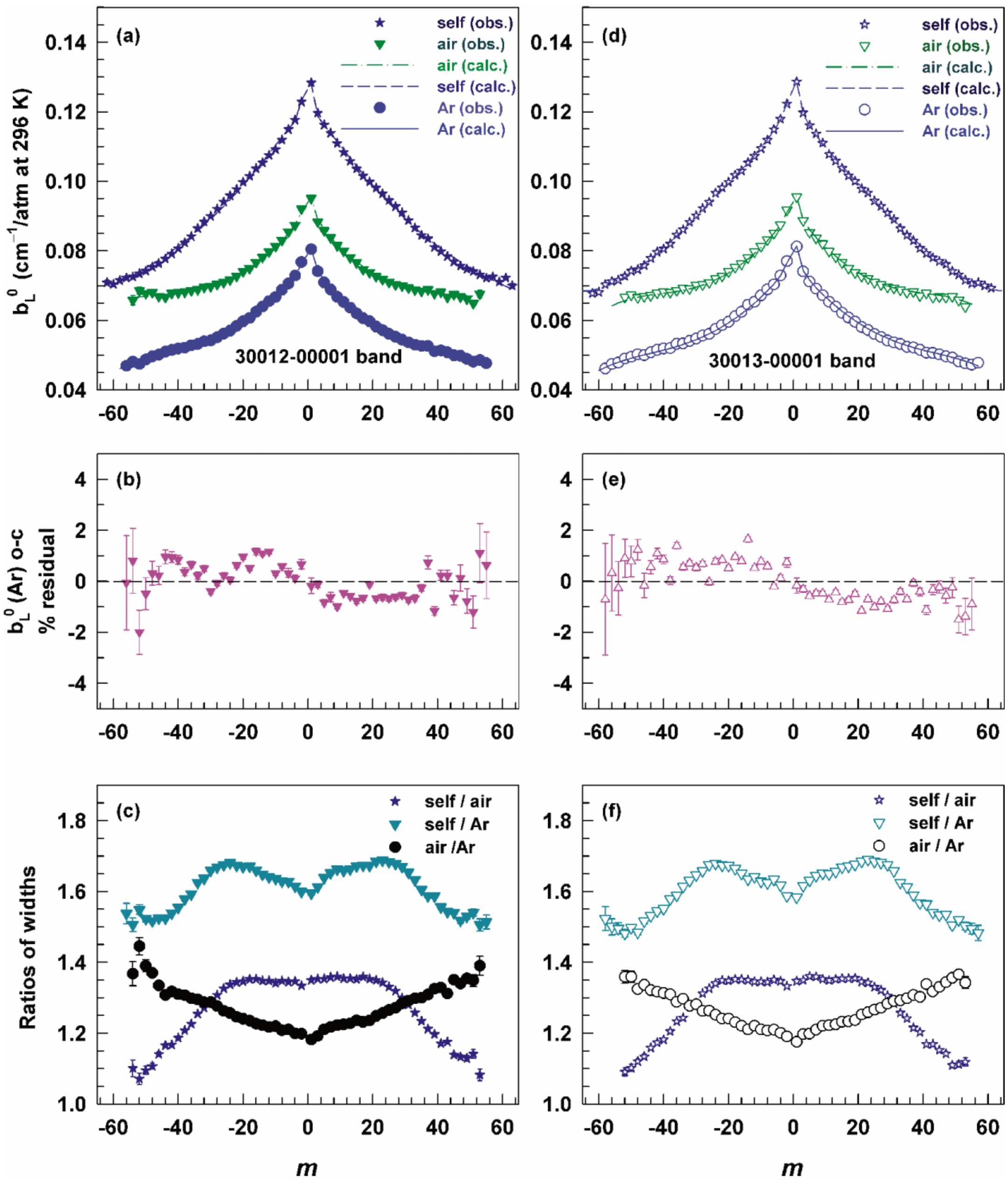

R-branch Ar-broadened half-width coefficients in both bands are calculated to be ∼ 1.02 ± 0.01. These small differences are responsible for the positive and negative percentage differences seen in Figs. 3*b* and 3*e*. There are hints of this P-branch–R-branch asymmetry in the self- and air-broadened half-width coefficients reported in refs. 4, 5, but the pattern is not as pronounced as it is for Ar-broadened half-width coefficients. The calculated half-width coefficients do not represent the measured data to its fullest accuracy, so the best values to use are the measured values.

The ratios of self- to air-, self- to Ar-, and air- to Ar-broadened half-width coefficients determined for 30012← 00001 and 30013←00001 bands as a function of *m* are plotted in Figs. 3*c* and 3*f*, respectively. These ratios vary with

Fig. 4. Comparison of Ar-shift coefficients. (*a*) Measured Ar pressure-shift coefficients for the 30012←00001 and the 30013←00001 bands of $^{16}O^{12}C^{16}O$ (cm^{-1}/atm at ~294 K) are plotted as a function of m. CO_2–Ar pressure-shift coefficients from Thibault et al. [13] for the $3\nu_3$ band are plotted for comparison. (*b*) Measured Ar pressure-shift coefficients for the 31112←01101 and 31113←01101 bands of $^{16}O^{12}C^{16}O$ (cm^{-1}/atm at ~294 K) are plotted as a function of *m*. Where error bars are not visible, the uncertainties are smaller than the size of the symbols used.

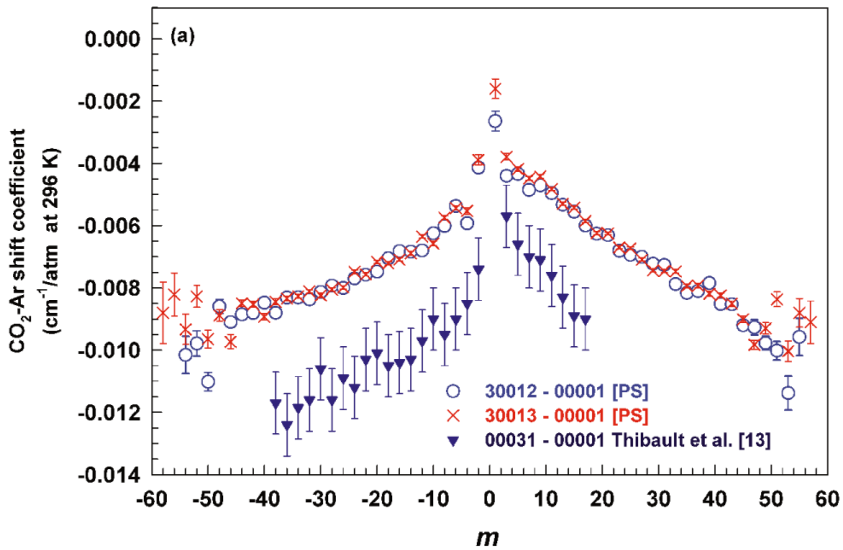

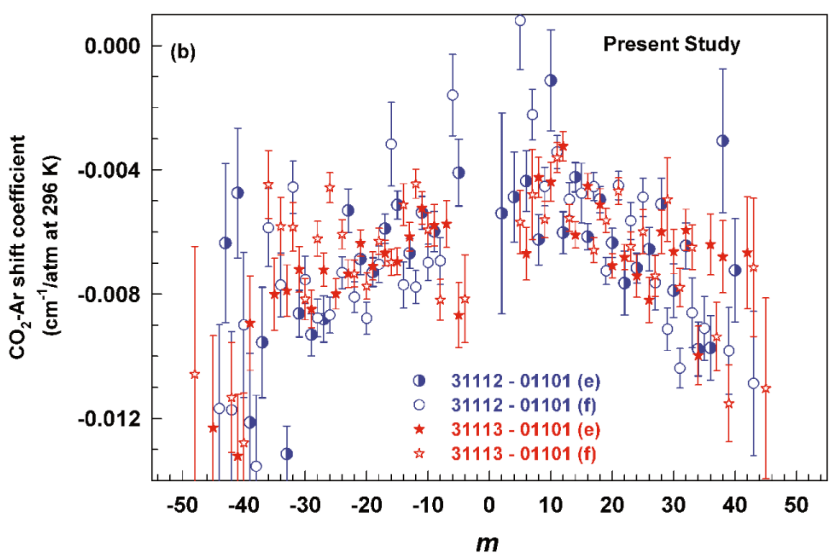

m, as also seen in Figs. 3*a* and 3*d*. The mean and standard deviations of these ratios (self- to air-broadening, self- to-Ar broadening, and air- to Ar-broadening) for the 30012←00001 band are found to be 1.26 and 0.09, 1.61 and 0.06, and 1.28 and 0.06, respectively. The ratios of the self- to Ar-broadened half-width coefficients have maxima near P28 and R28. The ratio increases from ~1.6 near the center of the band to ~1.7 near the maxima and then slowly falls off to ~1.55 toward higher-*J* transitions. Beyond the P48 and R48 lines, the ratios tend to increase slowly. The general patterns in the variations of self- to air- and self- to Ar-broadening with *m* are similar, although there is a shift in the self- to Ar-broadened half-width coefficients (higher) relative to those of self- to air-broadening. The pattern observed for the variations of air- to Ar-broadening with *m* is quite different from the other two cases; the ratio has a minimum of ~1.2 near the center of the band and gradually increases to 1.4 with higher *m* in both branches. Very similar values are obtained for the 30013←00001 band. Corresponding plots for the 30013←00001 band are displayed on the right-side panels of Fig. 3. Where error bars are not visible, the uncertainties are smaller than the size of the symbols used.

In Fig. 4, the experimental Ar-induced pressure shift coefficients (cm^{-1}/atm at ~294 K) as a function of *m* are plotted for transitions in the 30012←00001 and 30013←00001 and the 31112←01101 and 31113←01101 bands. The pressure-shift coefficients for the 30012←00001 and 30013←00001 bands are plotted in panel Fig. 4*a*, and those for the 31112←01101 and 31113←01101 bands in panel Fig. 4*b*. The transitions belonging to the 31112←01101 and 31113←01101 bands are weak, and the measured shift coef-

Fig. 5. Comparison of measured Ar pressure-shift coefficients. (*a*) The measured Ar-shift coefficients for the 30012←00001 band from present work are plotted as a function of *m* and compared with measurements for self- and air-shift coefficients from ref. 4. The experimental Ar-shift coefficients are fitted to the same empirical expression used in [2, 3] and the calculated Ar-shift coefficients are plotted by a solid curve. (*b*) The percentage differences between Ar-shift coefficients and the fitted curve are plotted as a function of *m*. (*c*) The differences (self-Ar) pressure-shift coefficients are plotted as a function of *m*. (*d*) the ratio of self- to Ar-shift coefficients are plotted as a function of *m*. The corresponding results obtained for Ar pressure-shift coefficients for the 30013←00001 band are displayed in (*e*)-(*h*).

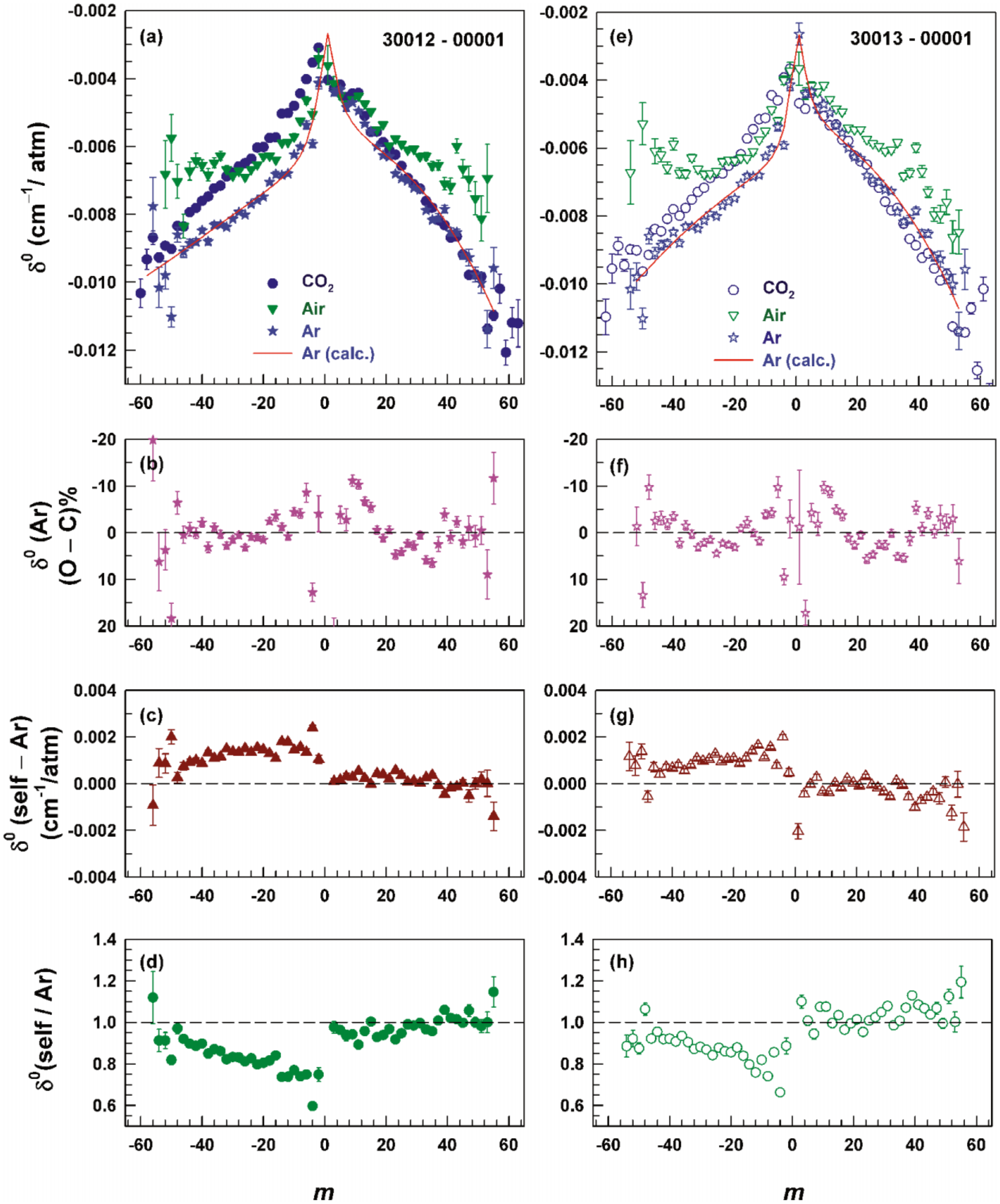

ficients therefore have larger uncertainties. In Fig. 4*a*, it is apparent that the shift coefficients in the bands from the ground state are significantly different in the P and R branches. For comparison, the Ar-induced shift coefficients in the $3\nu_3$ band by Thibault et al. [13] are compared with present measurements in Fig. 4*a*. Those pressure-shift coefficients are more negative than present values. The Ar pressure-shift coefficients for the 30012←00001 and 30013←00001 bands are all negative and range between ~ –0.002 and –0.011 cm^{-1}/atm at ~294 K. The Ar pressure-shift coefficients for the 31112←01101 and 31113←01101 bands are found to be slightly more positive near low *J*, although this may be due in part to the larger uncertainty in these measurements as noted above. The large scatter observed in both the Ar-broadened half-width (Fig. 2*b*), and especially the pressure-shift coefficients (Fig. 4*b*) for the hot bands, is because of the weak absorption of these lines.

In Figs. 5*a* and 5*e*, the measured δ^0(Ar) coefficients for the 30012←00001 and 30013←00001 bands are re-plotted as a function of *m* with the self- and air- shift coefficients

Fig. 6. Comparison of measured Ar-broadened off-diagonal relaxation matrix element coefficients and speed dependence in 30012←00001 and 30013←00001 bands. (*a*) Measured off-diagonal relaxation matrix elements (cm^{-1}/atm at 296 K) for Ar-broadening compared with previous measurements determined for self- and air-broadened off-diagonal relaxation matrix element coefficients [4, 5] plotted as a function of *m* for the 30012←00001 and 30013←00001 bands of $^{16}O^{12}C^{16}O$. (*b*) The measured speed dependence parameters in the P- and R-branch transitions of the 30012←00001 and 30013←00001 bands of $^{16}O^{12}C^{16}O$ are plotted vs. *m*. The speed dependence parameters determined from previous analyses [4, 5] of self- and air-broadening are also displayed for comparison purpose. The speed dependence parameter is assumed to be independent of broadening gas, and a single value is used to fit each transition (see text for details). Where error bars are not visible the uncertainties are smaller than the plot symbol.

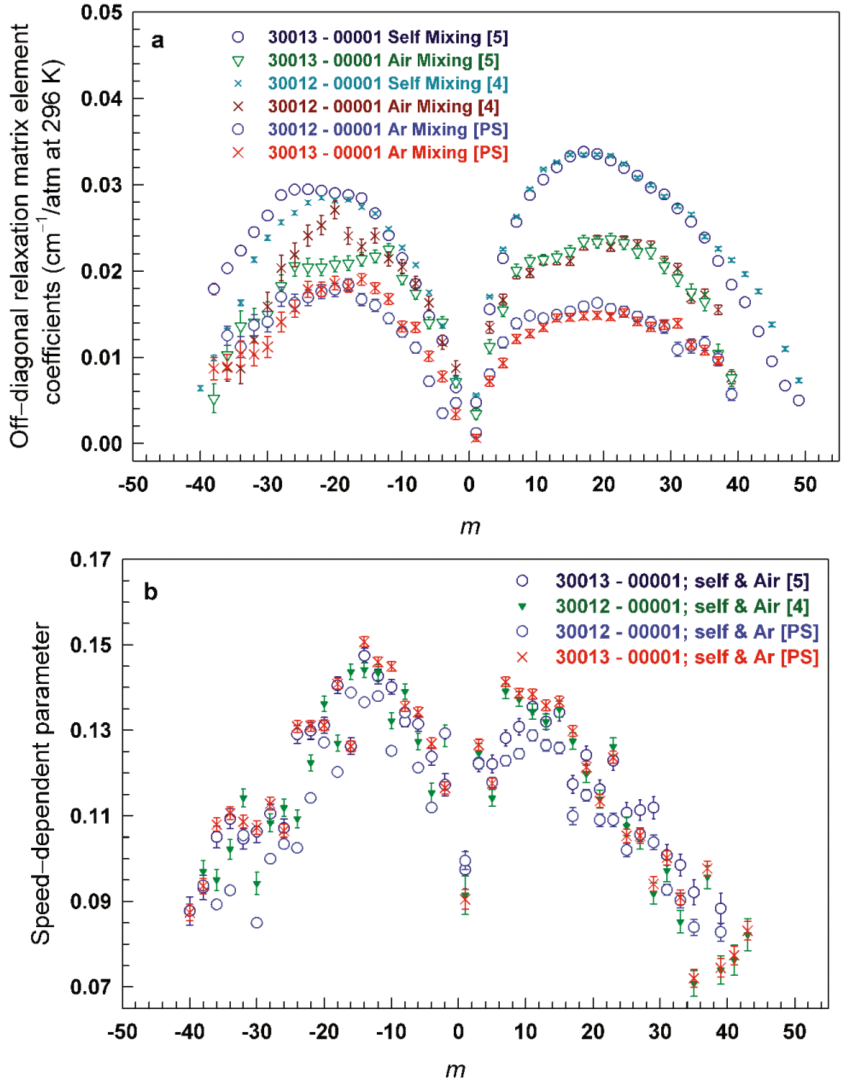

obtained previously [4, 5] for the same transitions. The measured Ar-shift coefficients are fitted to the same form of empirical function used by Toth et al. [2, 3], and the calculated values (for Ar shift coefficients) are shown by the solid curves passing through the measured points. The percentage differences δ^0(Ar) (obs.-calcd.), between the measured and empirically calculated pressure shift coefficients are plotted as a function of *m* in Figs. 5*b* and 5*f*. The measured and modeled values agree within ±5% with a few exceptions at low and high *J* values. The systematic nature of the point-to-point residuals, though, points to the fact that the modeled function does not fully match the measured shifts. Thus, the measured shifts should be used in preference to the modeled ones and the coefficients found for the fitted curve are not given. Figures 5*c* and 5*g* display the differences between self- and Ar-induced shift coefficients as a function of *m*. From Figs. 5*a* and 5*e*, it is apparent that the self- and Ar-induced shift coefficients follow fairly closely to each other in the R branch and there is a nearly constant shift between the self- and Ar-induced shift coefficients in the P branch; the Ar-induced shifts being slightly more negative than the self-induced shifts. Therefore, the self shift minus Ar shift in the R branch is close to zero all the way from R0 to R56, while in the P-branch side, there is ∼ +0.001 to +0.002 cm^{-1} difference in δ^0(self-Ar) from P2 to P56. It was not possible to find similar smooth variations in the shift coefficients as a function of *m* between air- and Ar-broadening. The dashed line corresponds to zero difference.

Figures 5*d* and 5*h* display the ratios δ^0(self and Ar) as a function of *m*. The results are almost a mirror image of those seen in the differences in the shifts in Figs. 5*c* and 5*g*. For example, in the 30012←00001 band, the ratio obtained in the R branch is between ∼0.95 and 1, while in the P branch the ratio varies from ∼0.7 to 1.0 from P2 to P56. The horizontal dashed lines in Figs. 5*d* and 5*h* correspond to a ratio of 1.0.

4.2. Ar line mixing and speed-dependent line shapes

We observed small, but persistent, systematic residuals in the multispectrum fits of Ar-broadened spectra similar to those attributed to line mixing and speed-dependent line shapes in our previous studies on self- and air-broadening [4, 5]. As done in refs. 4 and 5, we invoked line mixing by including nearest neighbor off-diagonal relaxation matrix elements in the multispectrum fit by the formulation of [33, 34], which define W_{ij}. This reduced the fitted residuals from a global standard deviation of 0.099% to 0.079%. However, some small systematic residuals remained under the line centers of the stronger transitions (P40-R40) of the 30012←00001 and 30013←00001 bands. These remaining residuals were removed by including speed dependence by the formulation of [34]. This further reduced the overall standard deviation of the fit from 0.079% to 0.076%. The fit residuals due to line mixing and speed dependence are different in appearance and hence distinguishable in our multispectrum fits. The effect upon the half-width coefficients by including these effects in the spectral line profile is to increase them by 2%–3%. The effect upon the pressure shift coefficients is to make them more negative by up to a few percent on the low wavenumber side of a P or R branch and up to a few percent less negative on the high wavenumber side. Near the center of the branch, the effect upon the shift coefficients is much smaller.

As an example, the final multispectrum fit interval for the 30012←00001 band is shown in Fig. 1. Similar to [4, 5], line mixing was considered only between the nearest neighboring lines in the P and R branches; all other off-diagonal relaxation matrix elements were fixed to zero. The measured off-diagonal relaxation matrix element coefficients (cm^{-1}/atm at 296 K) for the 30012←00001 and the 30013←00001 bands are listed in Table 6. The parameters determined for self-mixing and air line mixing [4] are also given in Table 6 for comparison. It is clear that the measured off-diagonal relaxation matrix element coefficients depend upon the broadening gas; vary significantly with *m* and are somewhat different in the P and R branches. The off-diagonal relaxation matrix element coefficients are the largest for self-broadening and smallest for Ar-broadening with air-broadening having intermediate values, similar to the trend observed for pressure-broadened half-width coefficients. The temperature dependences of the off-diagonal relaxation matrix elements for Ar-broadening were fixed to 0.75 to be consistent with the assumed temperature dependence exponents of pressure-broadened half-width coefficients. This introduced negligible errors in the measured line mixing parameters, since the present data were all obtained near room temperature (∼294 K).

The measured off-diagonal relaxation matrix elements and speed dependence parameters for the 30012←00001 and 30013←00001 bands are plotted as a function of *m* in Fig. 6. The off-diagonal relaxation matrix elements for self-, air-, and Ar-broadening are plotted in panel Fig. 6*a* and the speed dependence parameters for self- and air-, and self- and Ar-broadening in panel Fig. 6*b*. Similar to self- and air-broadening [4, 5], the off-diagonal relaxation matrix elements beyond m = 40 were fixed to 0.004 cm^{-1}/atm, and the speed-dependent parameters were fixed to 0.1 in the present analysis. We used a single speed dependence parameter for each transition in the multispectrum fit, since the speed dependence parameter is related to the temperature dependence of the half-width, and the same temperature dependence for both Ar- and self-broadening was assumed.

5. Conclusion

Experimental measurements of Ar-broadened half-width and Ar-induced pressure-shift coefficients at room temperature are reported for transitions in the 30012←00001 and 30013←00001 bands and for the associated hot bands transitions in 31112←01101 and 31113←01101. Systematic errors in the multispectrum nonlinear least-squares analysis used in the present study are minimized by using a Voigt line shape, modified to include both line mixing and speed dependence. The measured half-width and pressure-shift coefficients from the present study are compared with similar parameters recently obtained for self- and air-broadening [4, 5].

In the present work, the same set of self-broadened spectra included in recent previous studies [4, 5] are used. Air-broadened CO_2 spectra used in the previous analysis were substituted with Ar-broadened CO_2 data. The goal in this study was to keep the same level of accuracy in the various spectroscopic line parameters as in the previous study (self-broadening, self-induced pressure shift coefficients, self-line mixing; as well as line center positions and line intensities) and measure Ar-broadened half-width and Ar pressure-shift coefficients with the maximum possible accuracy. These new measurements of Ar-broadened half-width and Ar pressure-shift coefficients as well as line mixing due to Ar-broadening should provide the best possible values available so far for remote sensing of planetary atmospheres. Accurate low-temperature pressure-broadened half-width and shift coefficients will be of great importance to atmospheric studies.

Acknowledgments

The material presented in this investigation is based upon work supported by the National Science Foundation under Grant No. ATM-0338475 to the College of William and Mary. The research at the Jet Propulsion Laboratory (JPL), California Institute of Technology, was performed under contract with National Aeronautics and Space Administration. The authors express sincere appreciation to M. Dulick of NOAO (National Optical Astronomy Observatory) for the assistance in obtaining the data. The authors thank NASA's Upper Atmosphere Research Program for support of the McMath–Pierce laboratory facility.

References

1. R.A. Toth, L.R. Brown, C.E. Miller, V. Malathy Devi, and D.C. Benner. J. Mol. Spectrosc. **239**, 221 (2006). doi:10.1016/j.jms.2006.08.001.
2. R.A. Toth, L.R. Brown, C.E. Miller, V. Malathy Devi, and

D.C. Benner. J. Mol. Spectrosc. **239**, 243 (2006). doi:10.1016/j.jms.2006.08.003.
3. R.A. Toth, L.R. Brown, C.E. Miller, V. Malathy Devi, and D.C. Benner. J. Mol. Spectrosc. **246**, 133 (2007). doi:10.1016/j.jms.2007.09.005.
4. V. Malathy Devi, D.C. Benner, L.R. Brown, C.E. Miller, and R.A. Toth. J. Mol. Spectrosc. **242**, 90 (2007). doi:10.1016/j.jms.2007.02.018.
5. V. Malathy Devi, D.C. Benner, L.R. Brown, C.E. Miller, and R.A. Toth. J. Mol. Spectrosc. **245**, 52 (2007). doi:10.1016/j.jms.2007.05.015.
6. A. Predoi-Cross, A.V. Unni, W. Liu, I. Schofield, C. Holladay, A.R.W. McKellar, and D. Hurtmans. J. Mol. Spectrosc. **245**, 34 (2007). doi:10.1016/j.jms.2007.07.004.
7. A. Predoi-Cross, W. Liu, C. Holladay, A.V. Unni, I. Schofield, A.R.W. McKellar, and D. Hurtmans. J. Mol. Spectrosc. **246**, 98 (2007). doi:10.1016/j.jms.2007.08.008.
8. D.C. Benner, C.P. Rinsland, V. Malathy Devi, M.A.H. Smith, and D.A. Atkins. J. Quant. Spectrosc. Radiat. Transfer, **53**, 705 (1995). doi:10.1016/0022-4073(95)00015-D.
9. D. Crisp, R.M. Atlas, F.-M. Breon, L.R. Brown, J.P. Burrows, P. Ciais, B.J. Connor, S.C. Doney, I.Y. Fung, D.J. Jacob, C.E. Miller, D. O'Brien, S. Pawson, J.T. Randerson, P. Rayner, R.J. Salawitch, S.P. Sander, B. Sen, G.L. Stephens, P.P. Tans, G.C. Toon, P.O. Wennberg, S.C. Wofsy, Y.L. Yung, Z. Kuang, B. Chudasama, G. Sprague, B. Weiss, R. Pollock, D. Kenyon, and S. Schroll. Adv. Space Res. **34**, 700 (2004). doi:10.1016/j.asr.2003.08.062.
10. R.A. Washenfelder, G.C. Toon, J.-F. Blavier, Z. Yang, N.T. Allen, P.O. Wennberg, S.A. Vay, D.M. Matross, and B.C. Daube. J. Geophys. Res. **111**, D22, D22305 (2006). doi:10.1029/2006JD007154.
11. F.P.J. Valero and C.B. Suarez. J. Quant. Spectrosc. Radiat. Transfer, **19**, 579 (1978). doi:10.1016/0022-4073(78)90092-4.
12. C.B. Suarez and F.P.J. Valero. J. Mol. Spectrosc. **71**, 46 (1978). doi:10.1016/0022-2852(78)90074-7.
13. F. Thibault, J. Boissoles, R. Le Doucen, J.P. Bouanich, Ph. Arcas, and C. Boulet. J. Chem. Phys. **96**, 4945 (1992). doi:10.1063/1.462737.
14. M. Margottin-Maclou, A. Henry, and A. Valentin. J. Chem. Phys. **96**, 1715 (1992). doi:10.1063/1.462126.
15. R.A. Brownsword, J.S. Salh, and I.W.M. Smith. J. Chem. Soc., Faraday Trans. **91**, 191 (1995). doi:10.1039/ft9959100191.
16. F. Rachet, M. Margottin-Maclou, A. Henry, and A. Valentin. J. Mol. Spectrosc. **175**, 315 (1996). doi:10.1006/jmsp.1996.0037.
17. C.F. Roche, A. Ernesti, J.M. Hutson, and A.S. Dickinson. J. Chem. Phys. **104**, 2156 (1996). doi:10.1063/1.470971.
18. N.N. Filippov, J.-P. Bouanich, J.-M. Hartmann, L. Ozanne, C. Boulet, M.V. Tonkov, F. Thibault, and R. Le Doucen. J. Quant. Spectrosc. Radiat. Transfer, **55**, 307 (1996). doi:10.1016/0022-4073(95)00170-0.
19. R. Rodrigues, B. Khalil, R. Le Doucen, L. Bonamy, and J.-M. Hartmann. J. Chem. Phys. **107**, 4118 (1997). doi:10.1063/1.474789.
20. M.S. Wooldridge, R.K. Hanson, and C.T. Bowman. J. Quant. Spectrosc. Radiat. Transfer, **57**, 425 (1997). doi:10.1016/S0022-4073(96)00074-X.
21. L. Ozanne, Q. Ma, N. Van-Thanh, C. Brodbeck, J.-P. Bouanich, J.-M. Hartmann, C. Boulet, and R.H. Tipping. J. Quant. Spectrosc. Radiat. Transfer, **58**, 261 (1997). doi:10.1016/S0022-4073(97)00007-1.
22. C.F. Roche, A.S. Dickinson, A. Ernesti, and J.M. Hutson. J. Chem. Phys. **107**, 1824 (1997). doi:10.1063/1.474534.
23. R. Rodrigues, C. Boulet, L. Bonamy, and J.-M. Hartmann. J. Chem. Phys. **109**, 3037 (1998). doi:10.1063/1.476921.
24. B. Khalil, F. Thibault, and J. Boissoles. Chem. Phys. Lett. **284**, 230 (1998). doi:10.1016/S0009-2614(97)01412-7.
25. F. Thibault, J. Boissoles, C. Boulet, L. Ozanne, J.-P. Bouanich, C.F. Roche, and J.M. Hutson. J. Chem. Phys. **109**, 6338 (1998). doi:10.1063/1.477187.
26. J.-M. Hartmann, R. Rodrigues, Nguyen-Van-Thanh, C. Brodbeck, C. Boulet, R. Le Doucen, N. Lacome, and L. Bonamy. J. Chem. Phys. **110**, 7733 (1999). doi:10.1063/1.478723.
27. C.F. Roche, A.S. Dickinson, and J.M. Hutson. J. Chem. Phys. **111**, 5824 (1999). doi:10.1063/1.479878.
28. J. Buldyreva and M. Chrysos. J. Chem. Phys. **115**, 7436 (2001). doi:10.1063/1.1394941.
29. F. Thibault, B. Calil, J. Buldyreva, M. Chrysos, J.-M. Hartmann, and J.-P. Bouanich. Phys. Chem. Chem. Phys. **3**, 3924 (2001). doi:10.1039/b103625b.
30. S. Nakamichi, Y. Kawaguchi, H. Fukuda, S. Enami, S. Hashimoto, M. Kawasaki, T. Umekawa, I. Morino, H. Suto, and G. Inoue. Phys. Chem. Chem. Phys. **8**, 364 (2006). doi:10.1039/b511772k.
31. C. Boulet, J.-P. Bouanich, J.-M. Hartmann, B. Lavorel, and A. Deroussiaux. J. Chem. Phys. **111**, 9315 (1999). doi:10.1063/1.480031.
32. J.S. Li, K. Liu, W.J. Zhang, W.D. Chen, and X.M. Gao. J. Quant. Spectrosc. Radiat. Transfer, **109**, 1575 (2008). doi:10.1016/j.jqsrt.2007.10.014.
33. A. Lévy, N. Lacome, and C. Chackerian, Jr. Spectroscopy of the earth's atmosphere and interstellar medium. Academic Press, Inc. San Diego, Calif. 1992. p. 261.
34. D.C. Benner, V. Malathy Devi, C.E. Miller, and L.R. Brown. Manuscript in preparation. (2009).
35. L.S. Rothman, A. Barbe, D.C. Benner, L.R. Brown, C. Camy-Peyret, M.R. Carleer, K. Chance, C. Clerbaux, V. Dana, V. Malathy Devi, A. Fayt, J.-M. Flaud, R.R. Gamache, A. Goldman, D. Jacquemart, K.W. Jucks, W.J. Lafferty, J.-Y. Mandin, S.T. Massie, V. Nemtchinov, D.A. Newnham, A. Perrin, C.P. Rinsland, J. Schroeder, K.M. Smith, M.A.H. Smith, K. Tang, R.A. Toth, J.V. Auwera, P. Varanasi, and Y. Yoshino. J. Quant. Spectrosc. Radiat. Transfer, **82**, 5 (2003). doi:10.1016/S0022-4073(03)00146-8.
36. L.S. Rothman, D. Jacquemart, A. Barbe, D.C. Benner, M. Birk, L.R. Brown, M.R. Carleer, C. Chackerian, Jr., K. Chance, V. Dana, V. Malathy Devi, J.-M. Flaud, R.R. Gamache, A. Goldman, J.-M. Hartmann, K.W. Jucks, A.G. Maki, J.-Y. Mandin, S.T. Massie, J. Orphal, A. Perrin, C.P. Rinsland, M.A.H. Smith, J. Tennyson, R.N. Tolchenov, R.A. Toth, J.V. Auwera, P. Varanasi, and G. Wagner. J. Quant. Spectrosc. Radiat. Transfer, **96**, 139 (2005). doi:10.1016/j.jqsrt.2004.10.008.